International Journal of Wavelets, Multiresolution and Information Processing

IMAGE ERROR CONCEALMENT BASED ON QIM DATA HIDING IN DUAL-TREE COMPLEX WAVELETS

AMIT PHADIKAR

Department of Information Technology, MCKV Institute of Engineering, Liluah, Howrah, West Bengal, 711204, India.
amitphadikar@rediffmail.com

SANTI P. MAITY *

Department of Information Technology, Bengal Engineering and Science University, Shibpur, Howrah 711 103, India.
santipmaity@it.becs.ac.in

MALAY K. KUNDU

Machine Intelligence Unit & Center for Soft Computing Research, Indian Statistical Institute, Kolkata 700 108, India.
malay@isical.ac.in

Received (27th August 2010)
Accepted (7th January 2011)
Communicated by (Santi P. Maity)

Transmission of block-coded images through error prone radio mobile channel often results in lost blocks. Error concealment (EC) techniques exploit inherent redundancy and reduce visual artifacts through post processing at the decoder side. In this paper, we propose an efficient quantization index modulation (QIM) based data hiding scheme using dual-tree complex wavelet transform (DTCWT) for the application of image error concealment. The goal is achieved by embedding important information (image digest) as watermark signal that is extracted from the original image itself, and is used to introduce sufficient redundancy in the transmitted image. At the decoder side, the extracted image digest is used to correct the damaged regions. DTCWT offers three-fold advantages viz. (1) high embedding capacity due to inherent redundancy that leads to the better reconstruction of high volume missing data, (2) better imperceptibly after data embedding since it most closely captures human visual system (HVS) characteristics than conventional DWT and (3) better watermark decoding reliability. Simulation results duly support the claims and relative performance improvement with respect to the existing results.

Keywords: Error concealment; data hiding; DTCWT; Halftoning; QIM; image digest.

*Santi P. Maity, Dept. of Information Technology, Bengal Engineering and Science University, Shibpur, Howrah 711 103, India. Tel.: (+91)(+33) 2668-4561/62/63 Extn; 846 fax: (+91)(33) 2668- 2916. .

1. Introduction

Transmission of digital data over unreliable network, particularly through radio mobile channel, is vulnerable to transmission error. Transmission error in the radio mobile channel occurs not only due to random noise but also due to multi-path fading effect. As a matter of fact, block coded image and video suffer from block loss leading to the severe degradation on image and video quality[1]. Forward error correction (FEC), automatic repeat request (ARQ) and hybrid FEC/ARQ schemes may not be the preferable choice especially for the real time applications subject to transmission over channels with high error rates and/or with high propagation delay. Alternatively, error concealment (EC) techniques, through post processing rather than suffering from the burden of retransmissions and consequent delay, may be adopted as a viable alternative to reduce image distortion at the decoder side.

A large number of different methods for image and video error concealment are reported in literature [2−21]. Error concealment is normally done either in spatial or in transform domain like discrete cosine transform (DCT), discrete wavelets transform (DWT) etc. The wavelet transform, multiresolution analysis, and other space-frequency or space-scale approaches now become standard signal-processing tool for detection, de-noising, compression of multimedia signals, transient detection, turbulence analysis, waveform coding, geometric representation and sharp image transition such as edges and texture segmentation etc., a few applications to mention[22−26]. Research work is also going to develop newer wavelets bases like bandlet[25], curvelet[27−28], ridgelet[29], divergence and curlfree wavelets[30] etc in order to make them suitable for various typical applications. Due to its various attributes and introduction of new members in the family day by day, wavelets also become a natural choice from the beginning of digital watermarking research[31−36]. Recently, Maity et al[37] reported the scope of various wavelets in performance improvement of spread spectrum watermarking.

Typically two classes of schemes, namely data interpolation and data hiding either separately or in combined form are used to meet the goal of error concealment. We classify them here as non-data hiding and data hiding based error concealment methods, respectively. Pixel domain interpolation (PDI)[2], directional interpolation (DI)[3,4], projection onto convex sets (POCS)[5], maximally smooth recovery (MSR)[6], block matching[7], and neighborhood regions partitioned matching[8] or spectral domain like DCT and DWT[9] are the few well known techniques for error concealment that do not use data hiding. Those schemes work well in simplified loss scenarios where successfully received data are assumed to be reconstructed as loss-free form. However, this is often not the case in real scenario. Moreover, those schemes being complex and time consuming are not suitable for real time error concealment where the decoder may not have sufficient computation power or is done in online[10].

Another class of error concealment method that enables the decoder to conceal errors upon their detection is data hiding. Redundant information of important fea-

ture such as edge information[11] and motion vectors are embedded for onward error concealment. Liu and Li[10] are the first authors who use data hiding as an error control tool. They extract the important information in an image, like the DC (direct current) component of each 8×8 block, and embed it into the host image. Gir et al[12] propose an error concealment technique utilizing DWT for embedding macro block-based best-neighborhood-matching (BNM) information. Nayak et al[13] claim that the use of projection on convex sets (POCS) together with watermarking give better result in error concealment than the result of applying individual one. Carli et al[14] propose an error concealment technique where multiple copies of the watermarks are embedded within the MPEG stream prior to entropy coding and without increasing bit rate. Adsumilli et al[15] propose a robust error concealment algorithm of image and video frame using spread spectrum (SS) watermarking. Lin et al[16] propose a joint best-neighborhood-matching (BNM) and watermarking technique to restore lost blocks in the region-of-interest (ROI) and region-of-background (ROB), respectively. Wang et al[17] use Lagrangian relaxation and dynamic programming to design a data hiding scheme that improves the error resiliency of object-based video by adaptively embedding the shape and motion information into the texture data.

It is reported in several works that the processing of data inside our visual cortex resembles filtering by an array of Gabor filters of different directions and scales. Most of the data hiding methods usually use DCT or DWT as embedding domain since the current lossy compression standards are based on those two transforms. The characteristics of human visual system are also studied lot based on them. However, DCT as well as DWT suffer from the lack of directionality and shift invariance. The lacks of shift invariance means small shifts in input signal can cause big changes in the energy distribution of the coefficients. The poor directional selectivity for diagonal features of DWT is evident from the impulse responses of the filters of individual subbands (Fig. 1(a)). There is only one filter for representing diagonal features. As a result, the DWT produces higher perceptual error due to watermark embedding, as there is only one subband representing the two opposing diagonal directions. In other words, the increase in watermark embedding strength along a diagonal edge inevitably produces distortion oriented orthogonal to the edge. However, this extra component (distortion) is not masked by edge and results in a higher perceived error. The Gabor-like nature of the complex wavelet transform (CWT) filters approximate the human visual perception well, which allows the watermark energy to adapt closely to the host image's local activity and results imperceptible watermarking[39]. Moreover, the dual tree complex wavelets transform (DTCWT) allows higher capacity, for a given embedding distortion, than both the spatial and DWT domains[40]. The increased data hiding capacity in DTCWT can be exploited to embed large amount of important information in the host data. Subsequently this leads to the perfect reconstruction of the missing data. Lastly, DTCWT also does not suffer from blocky artifacts, which are present in block-based

transform like the DCT. To the best of our knowledge the use of DTCWT has not yet been explored by watermarking research community for the application to error concealment of digital image.

This paper proposes an error concealment scheme for digital images using quantization index modulation (QIM) based data hiding in DTCWT. QIM is chosen for data hiding as it provides considerable performance advantages over spread-spectrum (SS) and low-bit(s) modulation in terms of the achievable performance trade-offs among distortion, rate, and robustnes[41]. Moreover, popular correlation based detector of spread spectrum watermark is not effective in the presence of fading-like operation[42]. Fading is always present and cause the loss of blocks during transmission of image or video signal over the radio mobile channel. The goal of error concealment is achieved here by embedding some important information (image digest) extracted from the original image itself. Induced redundancy increases error resiliency in radio mobile channels suffered from high error rates and/or with high propagation delay. Halftoning technique is applied to obtain image digest from the low-resolution version of the image. Image digest may act as pilot signal and be used to estimate channel state information (CSI). The main contributions of our work are (1) selection of DTCWT transform for watermark embedding that leads to lower perceived error, since it resembles most closely to human visual system (HVS) than conventional DWT, (2) high embedding capacity due to redundancy offered compared to DWT leading to an improved performance for the better error concealment. Simulation results duly support those claims. Performance of the proposed scheme is also tested in Rayleigh-fading wireless channel.

The rest of the paper is organized as follows: Basic principles and the key features of DTCWT are outlined in Section 2. The proposed error concealment scheme is introduced in Section 3. Some simulation results are presented in Section 4. Finally, the paper is concluded in Section 5.

2. Basic Principles and Key Features of DTCWT

DTCWT is a recent inclusion to the DWT family. In general, DWT produces watermarked images which are visually better due to the absence of blocking artifacts. However, there are two drawbacks associated with DWT i.e.

(1) Lack of *shift invariance* which means that small shift in the input signal can cause major variation in the distribution of energy between DWT coefficients at different scale. This causes poor performance in watermark detection.
(2) Poor *directional selectivity* for diagonal features, because the wavelet filters are separable and real. This implies that the watermark may be optimally adapted to the local image activity, which reduces the maximum allowable watermark energy.

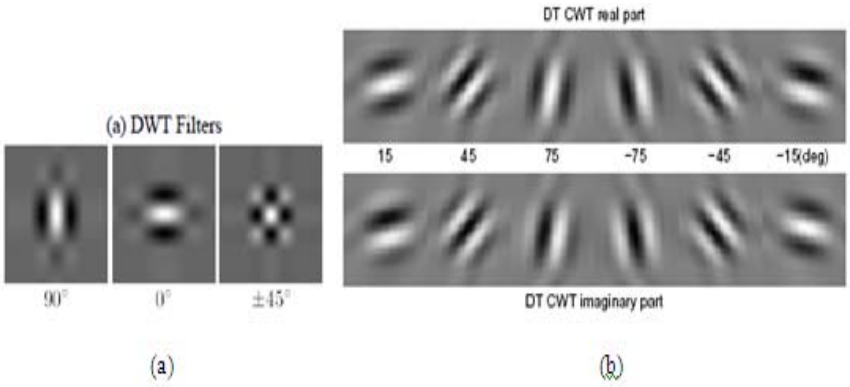

Fig. 1. Two dimensional impulse responses of the reconstruction filters (a) 2D DWT; (b) 2D DTCWT.

A straight forward way to provide shift invariance is to use the undecimated discrete wavelet transform (UDWT), but it has high computation requirements. On the other hand, when dealing with signals that have more than one dimension, the (DTCWT)[43,44,45] is a particularly valuable solution. This is due to perfect reconstruction of desirable properties that regular complex wavelets have: shift invariance and directional selectivity. Fig. 1(a) shows the two dimensional impulse responses of the reconstruction filters for the 2D (two-dimensional) DWT, while Fig. 1(b) shows the same for DTCWT. DTCWT achieves the *shift invariance* property with a redundancy factor of only 2^m for m-dimensional signals, which is substantially lower than the undecimated DWT. Moreover, the computation complexity of DTCWT is of $O(n)$. Fig. 2 shows the filter bank structure for 3-level DTCWT of a signal 'X'. Instead of having *one* wavelet tree with *complex* coefficients, the DTCWT uses two wavelets trees with real coefficients operating in parallel to give the *real* and *imaginary* parts of the wavelets coefficients. Each level of the transform produces complex coefficients that correspond to the output of six directional filters. If the level or ***scale*** of the filter outputs are denoted by $\boldsymbol{s}$ and the direction of the filter is denoted by $\boldsymbol{r}$, the set of highpass complex wavelet coefficients at level $\boldsymbol{s}$ can be written as

$$\begin{array}{l} y_{s,r}\left(u_s, v_s\right) = m_{s,r}\left(u_s, v_s\right) e^{j\theta_{s,r}(u_s,v_s)} \\ \quad For \;\; r = 1, ..., 6 \\ \quad\quad u_s = 0, ..., \frac{N}{2^S} - 1 \\ \quad\quad v_s = 0, ..., \frac{M}{2^s} - 1 \end{array} \tag{2.1}$$

where 'N' and 'M' are the row and the column size of the 2D multimedia signal like video frame/image. The variables u_s and v_s specify the location of the complex

coefficients in each subband. Fig. 3 shows the output structure for the six directional subbands at each level of two level decomposition of DTCWT.

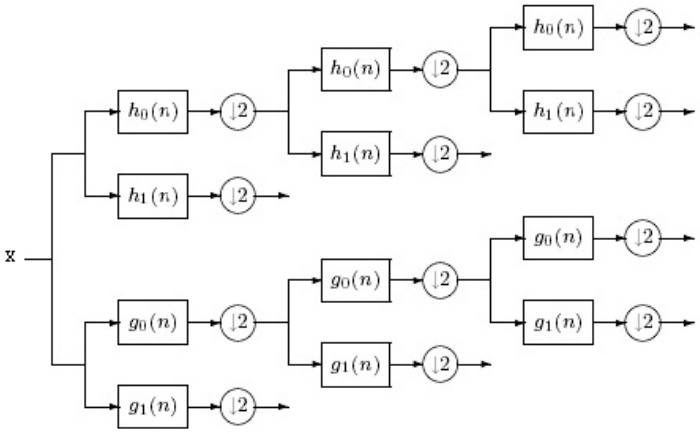

Fig. 2. Filter bank structure for a 3-level DTCWT.

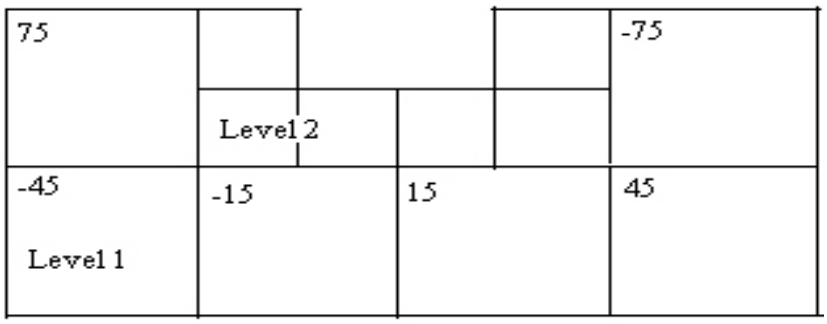

Fig. 3. Structure of the DTCWT coefficients for two level decomposition.

The mathematical form described in " 2.1" for DTCWT allows creation of correlation among different subbands. This form of correlation may be beneficial for data hiding on the coefficients and leads to better image visual quality of the watermarked data. To support the above argument, we calculate the entropy of different subbands for traditional DWT and DTCWT. The results are shown in Table 1. Numerical values are obtained as an average value of 100 independent experimentations conducted over large number of benchmark images having varied image characteristics. The equal and relatively higher numerical values of entropy for different orientations (subbands) of DTCWT based decomposition indicates that there exits lower correlation among the coefficients of subbands in DTCWT than the traditional DWT. In other words, a large entropy value indicates high randomness and

leads to higher data hiding capacity. Data hiding based error concealment exploits the advantages to embed more bits of watermark for a given embedding distortion.

Watermarking algorithms, in general, uses a pseudo random sequence. In QIM data embedding, the feature vectors of X, is quantized using a quantizer $Q_\Delta(\cdot)$, that is chosen from a family of quantizer based on the message bit (m), that is to be embedded[41]. The watermarked feature vector i.e. the watermarked coefficients $\tilde{X}$ is then given by:

$$\tilde{X} = Q_\Delta(X + d(m)) - d(m), \;\; m \in \{0, 1\} \tag{2.2}$$

where the symbol Δ is a fixed quantization step size, $d(.)$ is dither used for embedding watermark bit. The dither is generated using following rule.

$$d(0) = \{n \times \Delta\} - \Delta/2 \tag{2.3}$$

$$d(1) = \begin{cases} d(0) + \Delta/2 & if \; d(0) < 0 \\ d(0) - \Delta/2 & if \; d(0) \geq 0 \end{cases} \tag{2.4}$$

where the symbol n is a pseudorandom sequence. In general, $d(m)$ can be represented as:

$$d(m) = n \times a \tag{2.5}$$

where the symbol a is the scaling factor.

The watermarking process can be analyzed as communication channel, where the watermark is the signal and the host image is the noise. The simplest communication model is the additive white Gaussian noise (AWGN) channel that has the capacity C defined by[40,46]:

$$C = \frac{1}{2}\log_2\left(1 + \frac{S'}{N'}\right) \tag{2.6}$$

where S' and N' are the signal and noise variance, respectively. Unfortunately in a common watermarking scenario, the statistics of the noise is not Gaussian and the embedding rule is not always additive. In QIM scheme, the watermark is scaled before being added to the host signal. From " 2.2", we can write

$$\tilde{X} = Q_\Delta(X + a \times n) + (-a \times n) \tag{2.7}$$

and " 2.7" can be represented in additive watermarking form as:

$$\tilde{X} = \bar{X}' + w' \tag{2.8}$$

where $\bar{X}' = Q_\Delta\left(X + a \times n\right)/a$. The channel then becomes additive. Then the modified (i.e. inversely scaled) coefficients can be modeled as a two-Gaussian mixture with proportions p and $1-p$. The capacity is then given by[40]:

$$C = \frac{p}{2}\log_2\left(1 + \frac{\sigma_w^2}{\sigma_{X_1}^2}\right) + \frac{1-p}{2}\log_2\left(1 + \frac{\sigma_w^2}{\sigma_{X_2}^2}\right) \tag{2.9}$$

where σ_w^2 is the variance of w', while $\sigma_{X_1}^2$ and $\sigma_{X_2}^2$ are the variance of the host interference in the two-Gaussian mixtures, respectively. For DTCWT, the real and the imaginary parts are modeled separately as two-Gaussian mixture and the capacity are averaged. Table 2 lists both theoretical and experimental capacity for images in different domains[40]. We can see that the DTCWT domain has higher watermarking capacity than the DWT domain.

Table 1. Entropy of different subbands for normal DWT and DTCWT. BDE: before data embedding, ADE: after data embedding

	DWT			DTCWT	
Subbands	BDE	ADE	Subbands	BDE	ADE
Low-low(LL)	10.22	6.47	15	12	2.03
Low-high(LH)	8.20	3.65	-15	12	1.95
High-low(HL)	9.25	4.27	45	12	2.39
High-high(HH)	8.96	3.56	-45	12	2.11
			75	12	2.02
			-75	12	1.65
Average	9.16	4.48		12	2.03

Table 2. Theoretical (a) and experimental (b) capacities in kbits per image for the set of (512×512) test images. L=6, where the symbol L represents the length of dither.

Domain	Theoretical (a)	Experimental (b)
Spatial	11.60	7.20
DWT	22.00	16.40
DTCWT	36.80	20.40

Another reason for selecting DTCWT over traditional DWT is the better robustness over different common image and signal processing operations. It has been shown that the bit error rate (P_e) in binary watermark decoding is related to the standard deviation of the cover image coefficients[47] as follows:

$$P_e = \frac{2(M-1)}{M}\Upsilon\left(\sqrt{\frac{Ld_0^2}{4\sigma_x^2}}\right) \tag{2.10}$$

Table 3. The variance values for different subbands due to traditional DWT and DTCWT. BDE: before data embedding, ADE: after data embedding

	DWT			DTCWT	
Subbands	BDE	ADE	Subbands	BDE	ADE
Low-Low(LL)	13212000	13207000	15	245.37	330.30
Low-high(LH)	5391	5710	-15	113.26	124.77
High-low(HL)	70997	71144	45	3.672.5	3727.5
High-high(HH)	4573	4854	-45	972.00	1059.3
			75	322.00	352.39
			-75	108.63	121.21
Average	3323240	3322177		905.64	952.59

Table 4. Robustness performance in term of NCC; PSNR Attack (dB): A=10, B=20, C=30, D=40, E=50; Scaling Attack (Factor Scaling (%)): F=50, G=75, H=90, I=110, J=115; JPEG: K=25, L= 35, M=40, N=70, O=80, P=90; Median Filtering (Mask Size): Q=3×3, R=5×5, S=7×7, T=9×9; Removal of Line (Number of Line): U= 10, V=40, W=70, X=100; Rotation (Degree): Y=10, Z=15, A1=30, B1=35, C1=45.

	A	B	C	D	E	F	G	H	I	J
DWT	0.94	0.94	0.94	0.94	0.94	0.84	0.89	0.85	0.85	0.87
DTCWT	0.79	0.79	0.79	0.79	0.79	0.92	0.93	0.90	0.88	0.89
	K	L	M	N	O	P	Q	R	S	T
DWT	0.69	0.72	0.75	0.82	0.89	0.91	0.85	0.72	0.60	0.60
DTCWT	0.87	0.89	0.91	0.92	0.96	0.97	0.90	0.89	0.81	0.81
	U	V	W	X	Y	Z	A1	B1	C1	
DWT	0.78	0.85	0.81	0.81	0.80	0.78	0.75	0.74	0.75	
DTCWT	0.88	0.90	0.91	0.91	0.91	0.91	0.85	0.85	0.85	

where d_0 indicates step size (Δ), M indicates the total number of different step sizes, σ_x^2 is the variance of an image block, $\Upsilon(.)$ indicates the complimentary error function and L is the number of cover signal points over which a single watermark bit is embedded. It is seen from the simulation results (Table 3) over large number of images that the variance of DTCWT coefficients is much lower than the same statistical parameter for DWT coefficients. This in turn lowers the P_e for watermark decoding. Table 4 lists the comparative robustness performance in term of normalized cross correlation (NCC) for traditional DWT and DTCWT. Numerical values in Table 4 revel that DTCWT offers better robustness over DWT[48]. This supports the use of DTCWT based method for cover image decomposition. Moreover, it is also quite interesting to see from the results of Table 3 that the change in variance value due to data embedding for traditional DWT is, on an average 1063, while the same for DTCWT is 46.95. The change of variance due to data embedding is calculated when the value of step size (Δ) is 15 i.e. watermark power (WP)[49] is 12.73 dB. It is seen experimentally that the same change in variance value due to data embedding is possible to achieve in DTCWT domain using step size 43 i.e. watermark power (WP) of 12.73 dB. The results validate the fact that the fidelity

of watermarked image in DTCWT domain is high compared to traditional DWT domain for the same watermark power. The curves in Fig. 4 highlight the variation of variance values for different watermark power.

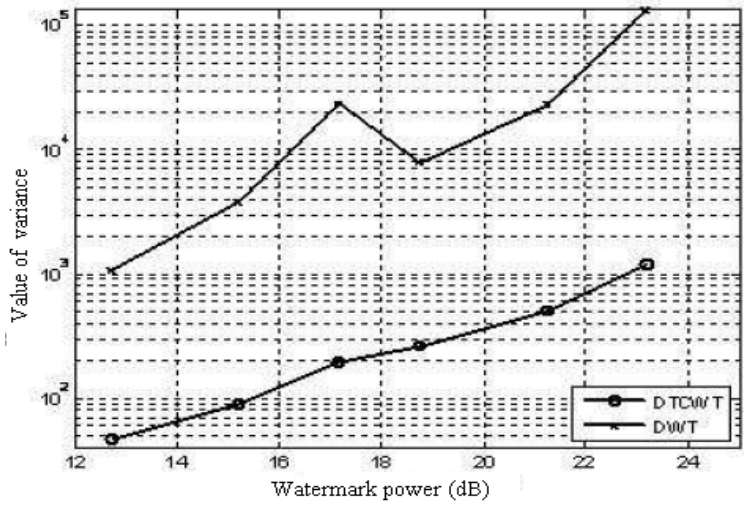

Fig. 4. Comparative change in variance value with different watermark powers.

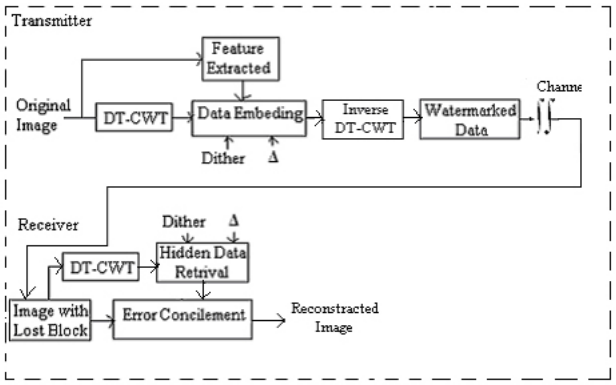

Fig. 5. Block diagram of the proposed error concealment scheme.

3. Proposed Image Error Concealment Scheme

The overall error concealment scheme consists of two stages: the data embedding stage at the transmitter and the error concealment stage at the receiver. The block

schematic representation of the proposed image error concealment scheme is shown in Fig. 5.

3.1. *Data embedding at transmitter:*

The objective of the transmitter is to embed the most important information (image digest) of the host image (h) into the image itself to generate a watermarked image (h') at the output. The inputs to the encoding process are the gray scale image, the owner key (K), and a secret key for the generation of dither that is used for watermark bit embedding. The encoding process is performed in different steps as follows:

Step 1: Image digest generation:

The whole image can not be inserted into the host due to capacity, fidelity and robustness trade-off. This in other way suggests embedding of an image digest, which is a compressed version of the original image. The image digest is generated using the following steps:

(a) The original image is resized so that its height and the width become half of the original one. The reduction in size is done in order to embed this information with sufficient amount of repetition into the various subbands of the DTCWT so that image digest can be recovered effectively.

(b) A halftoned image is then generated from the reduced size image using Floyd-Steinberg diffusion kernel D_{FS} given by[50,51]

$$D_{FS} = \frac{1}{16}\begin{bmatrix} 0 & 0 & 0 \\ 0 & P & 7 \\ 3 & 5 & 1 \end{bmatrix} \tag{3.1}$$

where P is the current pixel position and D_{FS} is typically applied on each (3×3) block of the reduced size image (m). The resulting halftoned image is denoted by 'W' which is of size $(N/2 \times N/2)$. The symbol 'N' denotes the number of row/column of the original image.

(c) The halftoned image (W) is permuted to get a noise-like image digest ($\tilde{W}$) using a secret key (K). On principle, the permutation of $\tilde{W}$ should cause the lost pixels of the cover to be separated as far as possible from the pixels where the corresponding bit of the image digest ($\tilde{W}$) is embedded. By doing so, the recovery of tamper region can be made more effective.

Step 2: Image transformation:

The original image is decomposed using n-level 2D-DTCWT. The number of levels of wavelet decomposition is implementation dependent; however, two (2) levels are demonstrated here for the experimentation. Simulation results (obtained through experimentation over large number of images) show that this number of decomposition levels is good enough to maintain acceptable performance of the proposed error concealment scheme through data hiding. Fig. 6(a) shows 2-level DWT of the 8-bits/ pixel house image tile, while Fig. 6(b) shows the same using DTDWT de-

composition. The ability of the DTCWT to separate the two diagonal directions is evident in the figure.

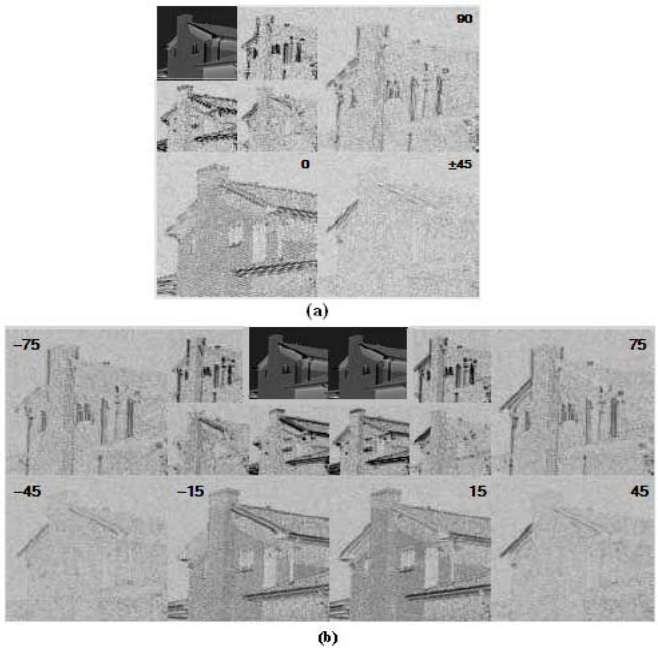

Fig. 6. (a): 2-level DWT of the 8-bit House image tile, (b): 2-level DTCWT of the 8-bit House image tile, Source[39].

Step 3: Data (image digest) embedding:
The image digest ($\tilde{W}$) is embedded into the DTCWT coefficients of the original image using the steps as described below:

(a): Selection of step size and generation of binary dither: Two dither sequences, each one of length L, are generated pseudo randomly using a *key* with step size (Δ) as follows:

$$d_q(0) = \{\Re(key) \times \Delta\} - \Delta/2 \;\; 0 \leq q \leq L-1 \tag{3.2}$$

$$d_q(1) = \begin{cases} d_q(0) + \Delta/2 & if \;\; d_q(0) < 0 \\ d_q(0) - \Delta/2 & if \;\; d_q(0) \geq 0 \end{cases} \tag{3.3}$$

where $\Re(key)$ is a random number generator. In the present scheme, the value of 'L' is chosen six(6), as one bit of image digest is embedded by modifying one coefficient of each orientation as shown in Fig. 1(b).

(b): Watermark bit insertion: The permuted halftoned image digest ($\tilde{W}$) is embedded in different subbands of 1^{st} level. Watermarking is done by modifying only the real part of the coefficients. The imaginary part is unaffected as experimentally it is seen that the embedding of watermark in this part makes the scheme very fragile. The q^{th} watermarked DTCWT coefficient S_q is obtained as follows:

$$S_q = \begin{cases} Q\left\{X_q + d_q(0), \Delta\right\} - d_q(0) & if\ \tilde{W} = 0 \\ Q\left\{X_q + d_q(1), \Delta\right\} - d_q(1) & if\ \tilde{W} = 1 \end{cases} \tag{3.4}$$

where X_q is the q^{th} DTCWT coefficient of the original image, Q is a uniform quantizer (and dequantizer) with step size Δ. After watermark embedding, inverse 2D-DTCWT (iDTCWT) is applied and the watermarked image (h') is formed.

3.2. *Error concealment at receiver*

The decoding process is just reverse to that of the encoding process. The inputs to the decoder are the received watermarked image and the secret keys. The keys are the same that were used at the time of watermark embedding for the generation of dither and permutation of image digest (watermark). In exigency of some blocks of the received signal (h') lost during transmission, the errors of image can be found and is concealed at the receiver using different steps as described follows:

Step 1: Step followed in 3(a) of the encoding process is performed at the decoder. The same key '$\Re(key)$ ' is used for the generation of the dither that is used at the time of image encoding.

Step 2: Generation of mask:
A binary mask (M) of size ($N \times N$) is generated from the received watermarked image with lost blocks. The usage of mask identifies the location of the lost pixel in a block. If $M(i,j) = 1$, the pixel in the mask is white. The location, where $M(i,j) = 1$, represents the lost pixel in the image. Now, its two level 2D-DTCWT is performed.

Step 3: Watermark extraction:
Received watermarked (h') image is decomposed by 2-level 2D-DTCWT to get h'_{r_l}, where r is the orientation/direction and the level $l \in \{1,2\}$. The image digest is extracted from the respective subbands that are used at the time of embedding. A watermark bit $\tilde{\tilde{W}}$ is decoded by examining real part of six DTCWT coefficients in different orientations of 1^{st} level using

$$\mathrm{A} = \sum_{q=0}^{L-1} \left(|Q(Y_q + d_q(0), \Delta) - d_q(0) - Y_q|\right) \tag{3.5}$$

$$B = \sum_{q=0}^{L-1} \left(|Q(Y_q + d_q(1), \Delta) - d_q(1) - Y_q|\right) \tag{3.6}$$

where Y_q is the q^{th} DTCWT coefficient of the received signal. The watermark bit $\tilde{\tilde{W}}(i,j)$ corresponding to a group of selected coefficients is now decoded using the following rule.

$$\tilde{\tilde{W}}(i,j) = \begin{cases} 0 \;\; if A < B \\ 1 \; otherwise \end{cases} \tag{3.7}$$

Step4: Spatial rearrangement of decoded watermark bits:
The extracted watermark ($\tilde{\tilde{W}}$) bits are then reverse permuted using key 'K' that was used at the time of encoding. This way the decoded watermark ($\hat{W}$) is obtained.

Step 5: Generation of low resolution image:
Low resolution image (m') is generated by applying inverse Floyd halftoning using $\hat{W}$ and the resized error image ($N/2 \times N/2$) as inputs. Then m' is resized to the size of original host image i.e. ($N \times N$) and is decomposed into n-level 2D-DTCWT.

Step 6: Error concealment:
The error concealment is done in two steps i.e. recovery of real lowpass subband and six complex highpass subbands for each level.

(a): Recovery of real lowpass subband: The real lowpass subband is recovered using the following rule.

$$h'_L{}^R = h'_L + M_L \odot m' \tag{3.8}$$

where $h'_L{}^R$ is the recovered real lowpass subband, h'_L is the real lowpass subband of the error image, M_L is the real lowpass subband of the binary mask (M) generated by step-1, and $\odot$ is the array multiplier.

(b) Recovery of complex highpass subbands: Afterward we zoom $h'_L{}^R$ to the size of the original image and then its 2 level 2D-DTCWT is performed. The error coefficients in the highpass subband of different orientation/direction of the received image are corrected using the following rule.

$$h'_H{}^R = h'_H \odot \bar{M_H} + M_H \odot h'_{L.Z}{}^R \tag{3.9}$$

where $h'_H{}^R$ is the recovered highpass subband, h'_H is the error highpass band, $h'_{L.Z}{}^R$ is the highpass subband of zoomed version of $h'_L{}^R$. The symbol M_H represents the mask where $M_H(i,j) = 1$ represents that the coefficients are lost in a corresponding

highpass subband. The symbol $\bar{M}_H$ indicates the complement of M_H.

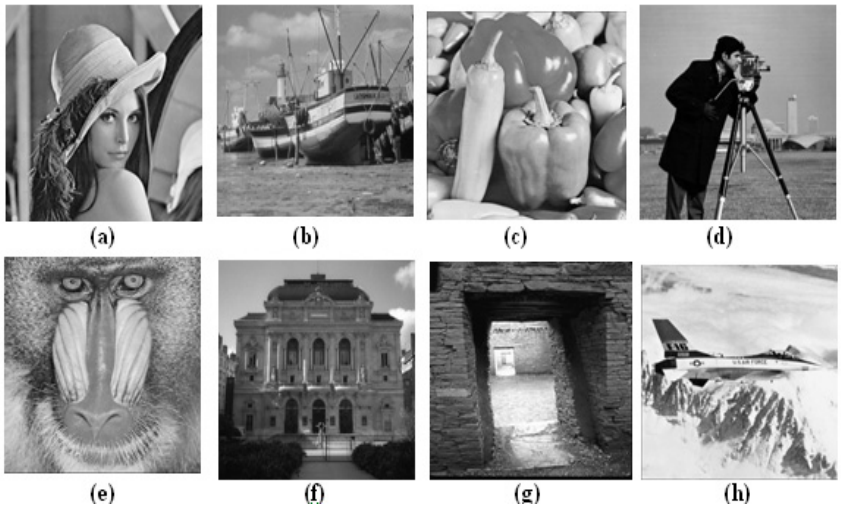

Fig. 7. Test images; (a): Lena, (b): Fishing boat, (c): Pepper, (d): Cameraman, (e) Baboon, (f): Opera, (g): Pueblo bonito, (h): F16.

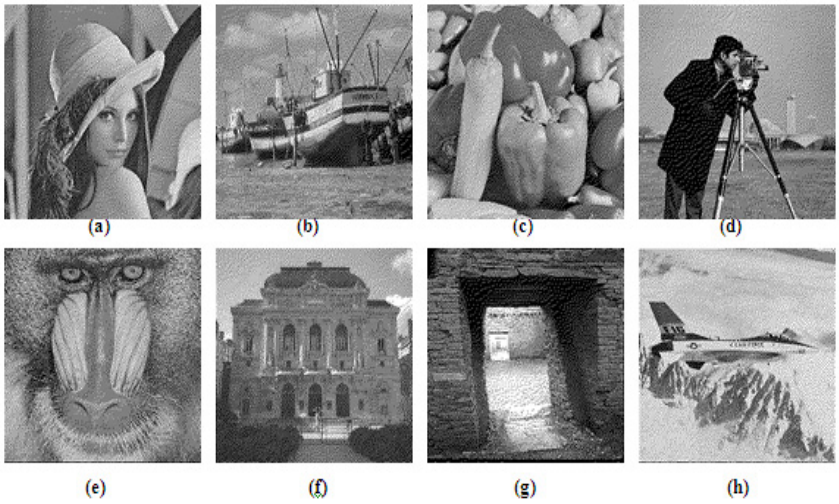

Fig. 8. Halftone images; (a): Lena, (b): Fishing boat, (c): Pepper, (d): Cameraman, (e) Baboon, (f): Opera, (g): Pueblo bonito, (h): F16.

4. Performance Evaluations

This section presents performance of the proposed error concealment scheme. Simulation is performed over a large number of benchmark images. However, results are reported here for eight popular test images; Lena, Fishing boat, Baboon, Cameraman, Pepper, Opera, Pueblo bonito and F16[52] as shown in Fig. 7. All the test images are of size (512×512), 8-bit/pixel gray scale image. The value of step size (Δ) taken into consideration is 20 i.e. watermark power (WP) is 15.23 dB. Peak-signal-to-noise-ratio (PSNR)[53] and mean-structure-similarity-index-measure (MSSIM)[54] are used here as distortion measure for the watermarked image under inspection with respect to the original image. Fig. 8 shows the image digest (halftoned images) extracted from the respective host image. Fig. 9 shows the watermarked images after embedding image digest to the respective host images, while Fig. 10 shows the extracted watermark (image digest) from the corresponding watermarked image. It is clear from Fig. 9 that the quality of the watermarked image in term of PSNR is almost same for various test images. Another interesting fact is also observed; a given watermark power though does not affect much on the visual quality (in PSNR values) for the watermarked images of all types but high numerical values of structural similarity are found for the images having high texture regions like Baboon and Pueblo bonito.

Fig. 9. Watermarked images (a): Lena, (b): Fishing boat, (c): Pepper, (d): Cameraman, (e): Baboon, (f): Opera, (g): Pueblo bonito, (h): F16. (P, M) above each image represents the PSNR (in dB) and MSSIM values of the image.

In the first set of experiments, we have studied the performance of the proposed

Table 5. PSNR and MSSIM after concealment of (8×8) & (16×16) block errors. EBS: Error blocks size, NBL: No of block loss, BC: Before Concealment, AC: After Concealment

Image	Error blocks		AC		BC	
	EBS	NBL	PSNR	MSSIM	PSNR	MSSIM
Lena	8×8	50	24.41	0.86	36.08	0.89
		75	22.96	0.84	35.62	0.88
		100	21.52	0.83	35.16	0.88
		125	20.68	0.83	35.10	0.87
		150	19.85	0.83	35.04	0.87
	16×16	50	19.22	0.85	35.96	0.91
		75	17.62	0.80	34.39	0.89
		100	16.02	0.76	32.83	0.88
		125	15.15	0.72	32.34	0.87
		150	14.28	0.68	31.85	0.87
Pepper	8×8	50	24.94	0.89	36.71	0.91
		75	23.19	0.87	36.20	0.91
		100	21.45	0.86	35.69	0.91
		125	19.83	0.84	35.41	0.91
		150	18.21	0.83	35.13	0.91
	16×16	50	18.52	0.84	33.36	0.90
		75	17.02	0.80	32.42	0.89
		100	15.52	0.76	31.48	0.88
		125	14.54	0.72	31.07	0.87
		150	13.57	0.69	30.67	0.87
Fishing Boat	8×8	50	24.25	0.91	36.42	0.93
		75	22.86	0.89	35.91	0.93
		100	21.48	0.88	35.41	0.93
		125	20.56	0.86	35.02	0.92
		150	19.64	0.85	34.63	0.92
	16×16	50	18.14	0.85	33.86	0.92
		75	16.63	0.81	32.70	0.90
		100	15.12	0.77	31.54	0.89
		125	14.30	0.74	30.67	0.88
		150	13.49	0.71	29.80	0.87
Camera man	8×8	50	24.96	0.91	36.81	0.96
		75	23.29	0.89	36.28	0.96
		100	21.47	0.87	35.79	0.96
		125	19.86	0.85	35.51	0.96
		150	18.27	0.83	35.15	0.96
	16×16	50	18.62	0.88	33.39	0.96
		75	17.12	0.84	32.52	0.94
		100	16.53	0.78	31.68	0.92
		125	15.54	0.76	31.12	0.91
		150	13.67	0.75	30.76	0.91
Baboon	8×8	50	24.44	0.87	36.91	0.97
		75	23.24	0.86	36.78	0.97
		100	22.60	0.85	35.79	0.97
		125	19.93	0.83	35.61	0.96
		150	18.71	0.83	35.53	0.95
	16×16	50	18.62	0.87	33.86	0.96
		75	17.72	0.82	32.92	0.92
		100	16.52	0.78	31.88	0.89
		125	15.54	0.74	31.67	0.88
		150	14.57	0.73	30.77	0.87
F16	8×8	50	24.96	0.86	36.73	0.92
		75	22.19	0.86	36.22	0.92
		100	22.45	0.85	36.69	0.92
		125	20.83	0.83	35.48	0.92
		150	19.21	0.82	35.03	0.92
	16×16	50	19.52	0.85	33.26	0.91
		75	17.82	0.81	32.13	0.90
		100	15.72	0.77	31.38	0.89
		125	14.64	0.73	31.01	0.88
		150	13.47	0.70	30.47	0.87
Pueblo bonito	8×8	50	24.15	0.92	36.12	0.95
		75	22.46	0.91	35.71	0.95
		100	21.28	0.90	35.11	0.95
		125	20.36	0.88	34.82	0.94
		150	19.24	0.87	34.23	0.94
	16×16	50	18.10	0.87	33.26	0.94
		75	16.33	0.83	32.30	0.92
		100	14.72	0.79	31.24	0.91
		125	14.10	0.76	30.37	0.90
		150	13.19	0.73	29.50	0.89
Opera	8×8	50	24.94	0.90	36.61	0.92
		75	23.19	0.88	36.01	0.92
		100	21.45	0.87	34.99	0.92
		125	19.83	0.85	35.11	0.91
		150	18.21	0.84	34.93	0.91
	16×16	50	18.51	0.85	33.16	0.91
		75	17.02	0.81	32.22	0.90
		100	15.12	0.77	31.18	0.89
		125	14.24	0.73	31.07	0.88
		150	13.17	0.70	30.47	0.88

error concealment scheme for lost or error blocks of different sizes like (8×8) and (16×16). The numbers of lost blocks vary from 50 to 150. Performance results of the proposed error concealment scheme are given in Table 5. Numerical values shown in Table 5 indicate that the improvement in PSNR values due to the proposed error concealment method are, on an average, 12 dB, 13 dB, 14 dB, 15 dB and 16 dB for the number of loss blocks 50, 75, 100, 125 and 150, respectively with the size of loss block (8×8). The similar improvement in PSNR values are of the order of 15 dB, 15.5 dB, 16 dB, 16.5 dB and 17 dB for the number of lost blocks 50,75, 100, 125 and 150, respectively with the size of loss block (16×16). Numerical values highlight that the proposed error concealment scheme is quite effective even for the large number of lost blocks with large size. This improvement is achieved due to the redundancy in number of subbands and sparse characteristics in DTCWT coefficients.

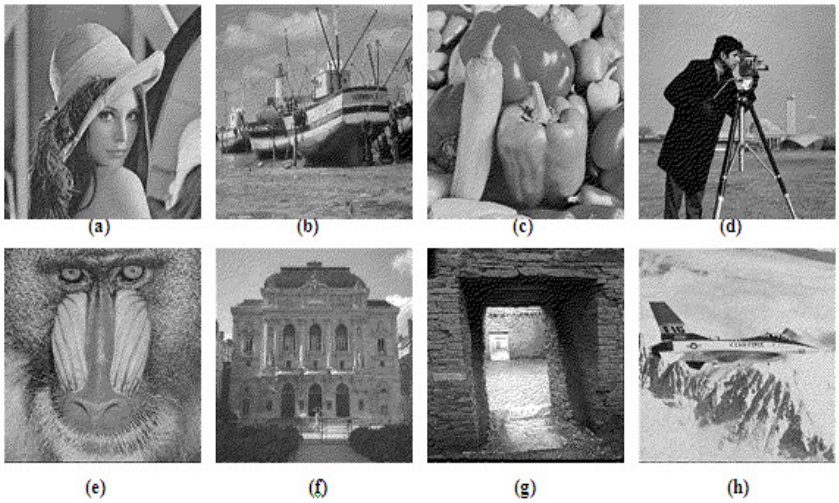

Fig. 10. Extracted watermark from (a): Lena, (b): Fishing boat, (c): Pepper, (d): Cameraman, (e): Baboon; (f): Opera, (g): Pueblo bonito, (h): F16.

Figs. 11(a)-11(d) show the error images having lost block of size (8×8). Figs. 11(e)-11(h) are the error concealed images of Figs. 11(a)-11(d), respectively. Figs. 12(a)-12(d) show the error images having block size (16×16). Figs. 12(e)-12(h) are the error concealed images of Figs. 12(a)-12(d), respectively. We also test our scheme for continuous block loss over a region. Fig. 13(a) shows the error image having continuous block loss, while Fig. 13(b) shows the error concealed image of Fig. 13(a). It is clear from Fig. 13(a) and Fig. 13(b) that proposed scheme recovers

image effectively even for the continuous block loss.

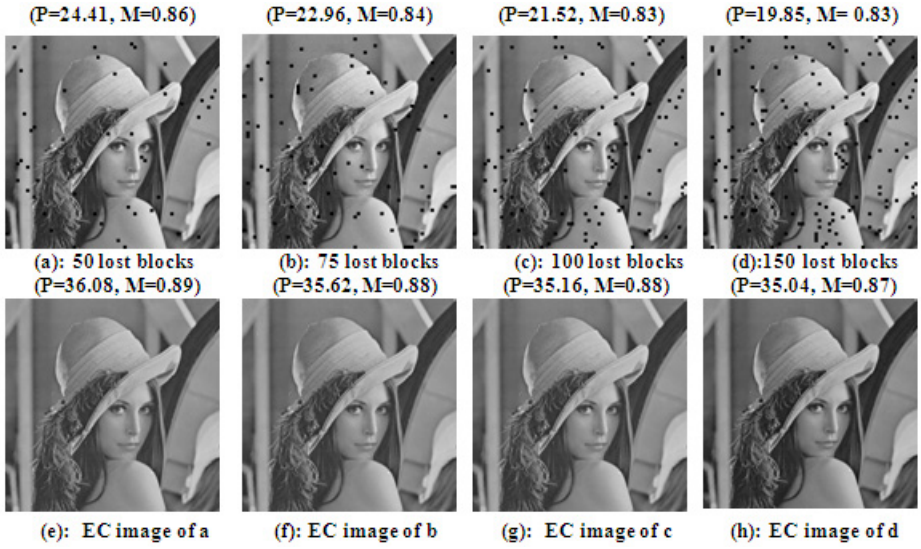

Fig. 11. (a)-(d) Received images with (8×8) size block loss; (e-h) error concealed images (e-h). (P, M) above each image represents the PSNR (in dB) and MSSIM values of the image

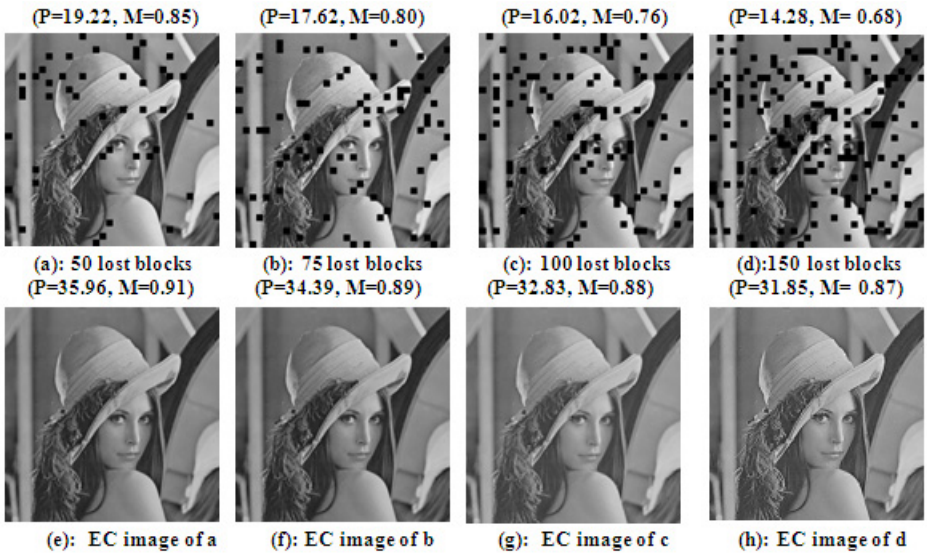

Fig. 12. (a)-(d) Received images (16×16) size block loss and (e-h) error concealed images (e-h). (P, M) above each image represents the PSNR (in dB) and MSSIM values of the image.

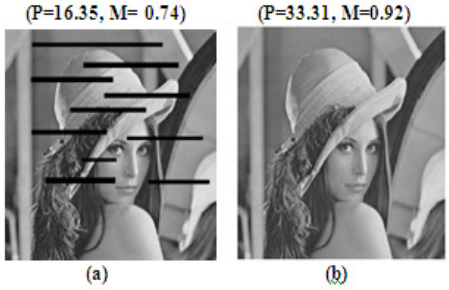

Fig. 13. (a) Damaged image; (b)restored image. (P, M) above each image represents the PSNR (in dB) and MSSIM values of the image.

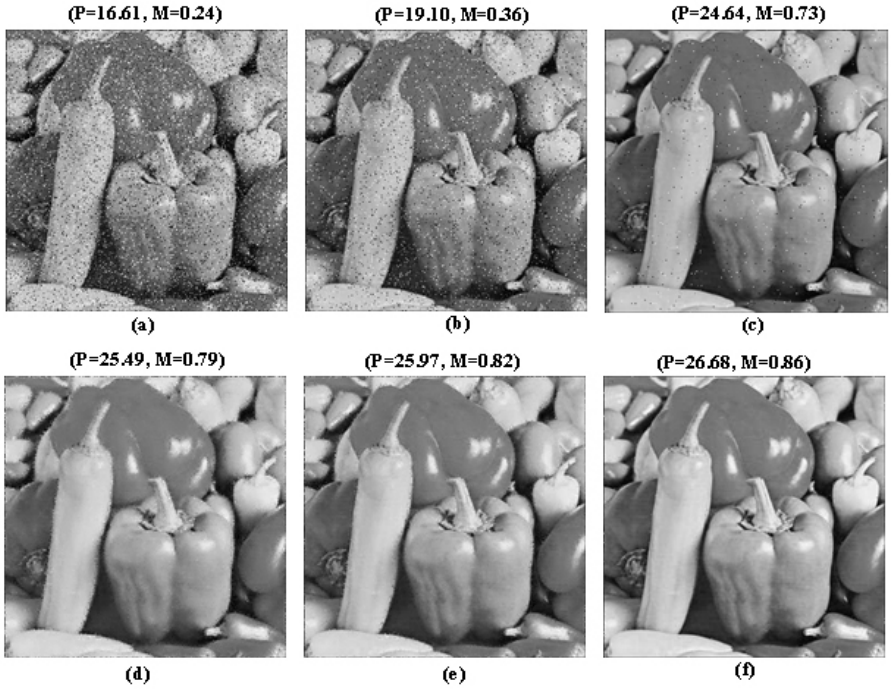

Fig. 14. Results under fading: (a) SNR= 1 (dB); (b) SNR= 3 (dB); (c) SNR= 7 (dB); (d) EC of a; (e) EC of b; (f) EC of c. EC: Error Concealment.

In order to show the effectiveness of the proposed error concealment method over fading channel, we simulate our test for different channel conditions. Data transmission is accomplished using multicarrier code division multiple access (MC-CDMA)[55,56] through Rayleigh fading with different SNR. Rayleigh fading is considered as it the widely used frequency selective fading model. The small value of SNR

Table 6. Performance in BER over Rayleigh fading wireless channel.

Channel SNR (dB)	1	3	7
BER	5.8×10^{-2}	2.20×10^{-2}	2.0×10^{-3}

Table 7. Experimental results under fading. EC: Error Concealment.

Channel SNR (dB)		1	3	7
Before EC	PSNR (dB)	16.61	19.10	24.64
	MSSIM	0.24	0.36	0.73
After EC	PSNR (dB)	25.49	25.97	26.68
	MSSIM	0.79	0.82	0.86

represents that the channel is under deep fade, while high value of SNR represents the reverse. Different bit error rate (BER) values at SNR=1 dB, SNR=3 dB and SNR=7 dB under Rayleigh fading are shown in Table 6. In wireless transmission, harsh conditions[57] are often occurred due to very high bit error rates (BER) in the order of 10^{-1} to 10^{-3}. Performance results of the proposed error concealment scheme are given in Table 7. Numerical values show that relatively high degree of improvement in quality i.e. PSNR (dB) and MSSIM values are possible to achieve through error concealment, when wireless channel condition is poor (i.e. high BER or low SNR). It is reasonable as better wireless channel condition offers better quality of the received image signal, which in turn does not provide scope of further improvement through error concealment. Figs. 14(a)-14(c) show received 'Pepper' images after passing through the fading channel for SNR=1 dB, SNR =3 dB, and SNR=7 dB, respectively. Figs. 14(d),(e) and 14(f) show various error-canceled images of Figs. 14(a)-14(c), respectively. Experimental results shown in Fig. 14 suggest that the proposed error concealment scheme is quite effective for the slow fading as well as for the wireless channel suffered by deep fades.

The algorithm developed can be made use to design an adaptive transmission scheme through the estimation of channel parameters (embedded watermark acts as pilot signal without effecting bandwidth and synchronization problem like the existing pilot based system). The quality of the extracted image digest will indicate the current status of the channel condition. When the quality of the error concealed image goes below the acceptable level (which is also reflected by the relative quality of the extracted image digest), a feedback information from the receiver to the transmitter to be sent indicating that the channel is under deep fade and current data rate is not well suited. The data transmission rate may be lowered for sometimes so long the quality of the error concealed image goes above the acceptable threshold level. In fading, corrupted pixels are shown by white and black spots. The present scheme uses two stage error detection technique proposed in[58] to find

corrupted pixel.

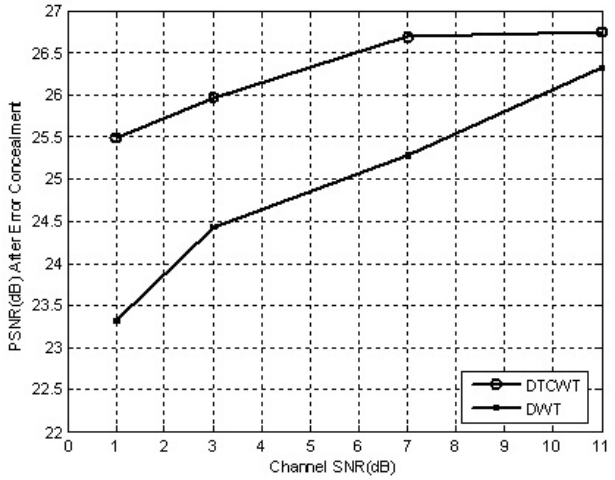

Fig. 15. Quality in term of PSNR (dB) for the error concealed image using DWT and DTCWT.

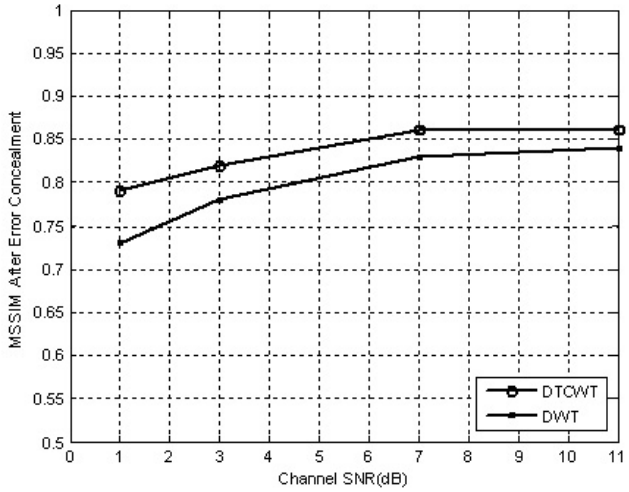

Fig. 16. Quality in term of MSSIM for the error concealed image using DWT and DTCWT.

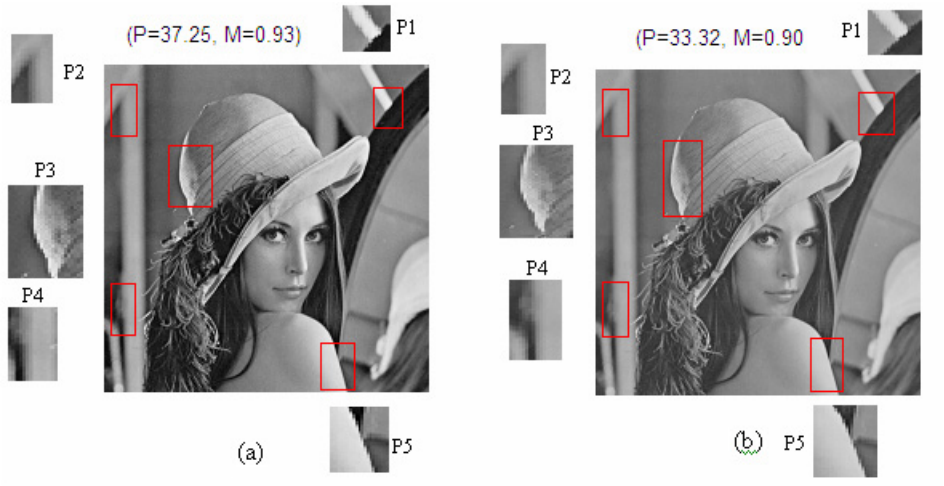

Fig. 17. Watermarked images (a): DTCWT; (b): DWT.

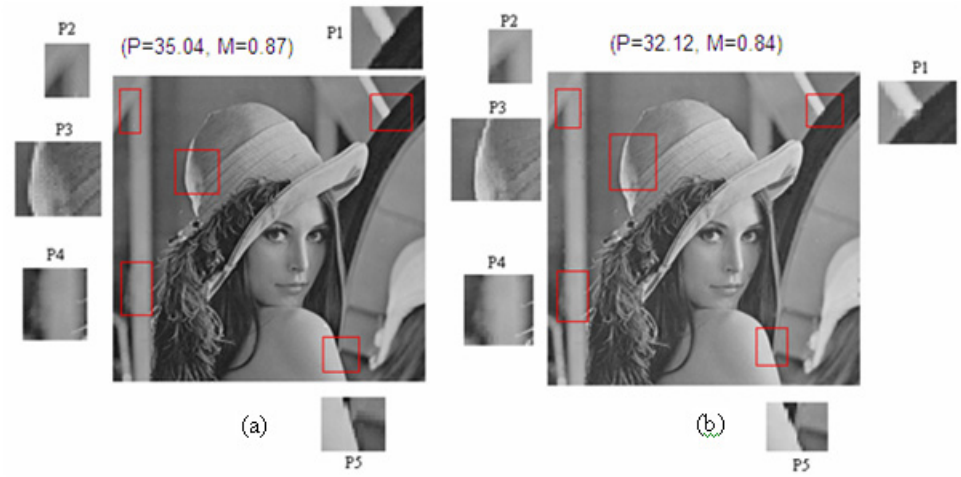

Fig. 18. Reconstruction of edge information of 150 blocks loss with size (8×8), (a): DTCWT; (b): DWT.

We have also studied the performance of the proposed scheme when image digest is embedded both in traditional DWT and DTCWT domain. The quality in term of PSNR (dB) and MSSIM of the error concealed images are presented through graphical plots shown in Figs. 15 and 16, respectively. Each point on the curves is obtained as the average value of 100 independent experimentations conducted over large number of benchmark images. Figs. 15 and 16 show the effectiveness of DTCWT for error concealment. This is due to the fact that DTCWT can distinguish between opposing diagonal features, because there are separate filters oriented at

Table 8. PSNR and MSSIM for watermarked image for different watermark power.

WP (dB)	9.21	15.23	18.75
PSNR (dB)	43.44	37.25	34.07
MSSIM	0.98	0.93	0.88

±45 degree. In other words, good directional selectivity for diagonal features of DTCWT offers low distortion due to data embedding at the edge point. When the edge orientations are of ±15 or ±75 degrees, the DTCWT offers better results than the DWT. This can also be visualized through a close look on P1 of Fig. 17 (a) and 17 (b). It is also clear from Figs. 18 and 19 that good directional selectivity offers better reconstruction of edge information over the traditional DWT after error concealment. From Figs. 18 and 19 it is clear that when the edge orientations are of ±15 or ±75 degree, the DTCWT offers better results than DWT. This can also be visualized through the subjective close look on Fig. 18 (P1) and 19 (P1).

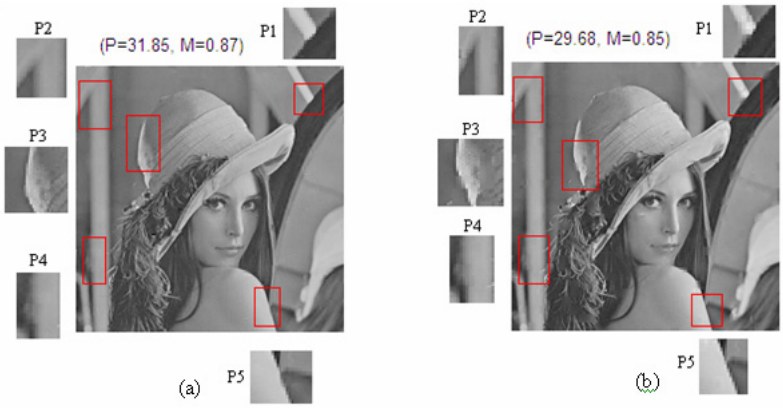

Fig. 19. Reconstruction of edge information of 150 blocks loss for size (16×16) (a): DTCWT; (b): DWT.

The effectiveness of the proposed scheme is also studied in case of scalable transmission. At the time of simulation, the watermarked image is coded at different bit rate (bit/pixel) and is transmitted over the channel. Fig. 20 shows the effectiveness of the use of DTCWT over DWT, when 150 (8×8) blocks are received with error.

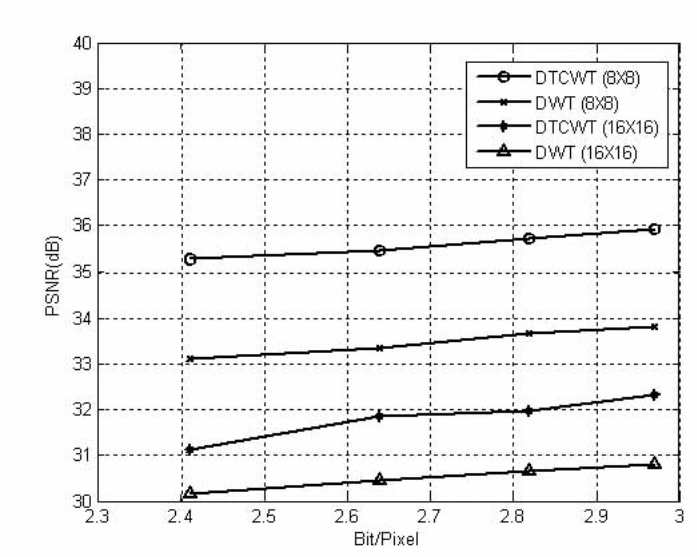

Fig. 20. Effectiveness of the use of DTCWT over DWT for error concealment during scalable transmission.

We also study the effect of different watermark powers (WP) on the relative gain/loss in performance for error concealment. The watermark power[49] is defined as:

$$WP = 10 \log_{10} \frac{\Delta^2}{12} dB \tag{4.1}$$

where the symbol Δ corresponds to the step size used for watermarking. Table 8 shows the relative visual qualities of the watermarked images for different watermark powers obtained through different step sizes. Respective MSSIM values are also reported in order to have an idea about the loss in structural information due to the variation of watermark powers. Figs. 21 and 22 show the graphical representations of PSNR and MSSIM values, respectively for the watermarked images with different number of lost blocks along with their various sizes. Figs. 23 and 24 show the relative improvement in quality after error concealment with respect to PSNR (dB) and MSSIM for different watermark power. Graphical representations reflect the fact that when watermark embedding power is relatively high and the size of the lost block is also large, the proposed data hiding based error concealment offers improvement in visual quality of ~ 15 to ~ 17 dB. It is also interesting to see from the results of Figs. 23 and 24 that although for a given watermark power and for a fixed size of loss block, the relative improvement in visual quality in PSNR does not vary much with the increase in number of lost blocks varying from 50 to 150 but significant improvement in structural information is found with the loss of more

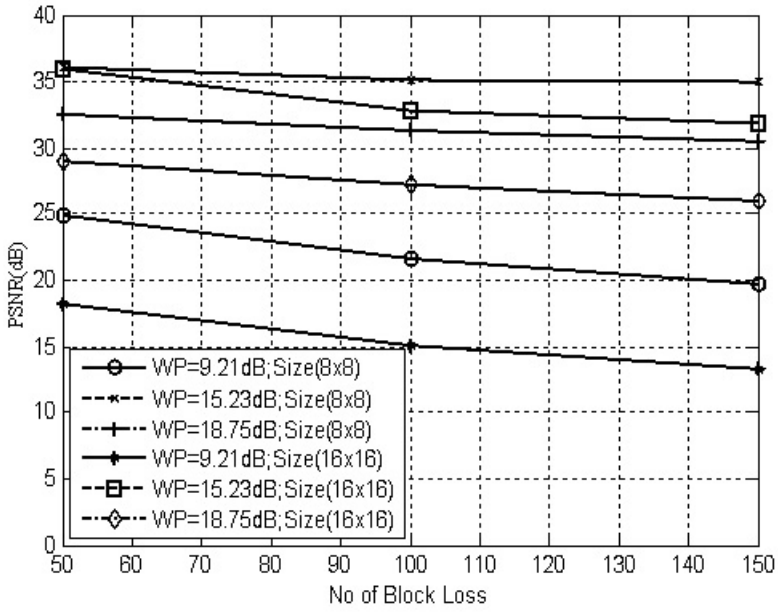

Fig. 21. PSNR (dB) after concealment of lost blocks for different watermark power (WP) in dB.

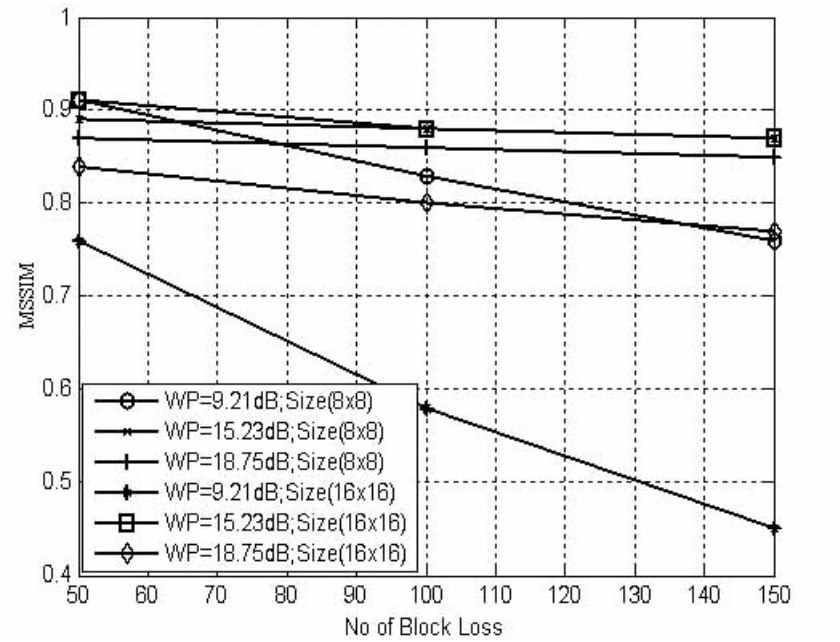

Fig. 22. MSSIM after concealment of lost blocks for different watermark power (WP) in dB.

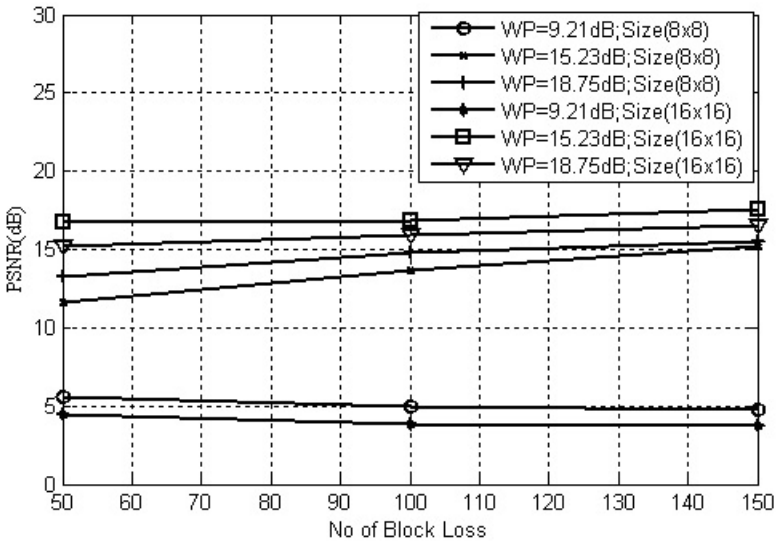

Fig. 23. Relative improvement in PSNR (dB) after concealment of lost blocks for different watermark power (WP) in dB.

A. Relative performance of non-data hiding and data hiding based error concealment:

Performance of the proposed method is compared with both non-data hiding[4,7,19,21] and data hiding based[12,18,20] methods intended for the application of error concealment. It is observed from the results of Table 9 that our method offers better PSNR values even if packet loss rate (PLR) increases to 30%. From Table 9 it is clear that when PLR is low, non-data hiding based error concealment methods offer similar performance like data hiding based approaches. But, the former (non-data hiding based) results in low improvement in quality at high burst error condition, as most of the surrounding blocks may be lost. Data hiding based scheme takes the benefits of redundancy, conceals the error quite effectively in burst error condition, and improves overall quality. Similarly, we also compare the result of the proposed method with the work reported in[12,18,20]. It is observed from the results in Table 9 that our method offers better results at high data loss condition as DTCWT offers high embedding capacity due to more number of subbands compared to normal DWT. Numerical results shown in Table 9 suggest that the proposed error concealment scheme may be thought as a viable alternative of continuous bit error as well as burst error to improve reliability in data transmission

Table 9. Comparison with other methods. The numerical values in Table 9 shows the PSNR (dB) of error concealed image.

PLR	3%	5%	10%	15%	20%	25%	30%
Lee et al[21] (2004)	31.12	26.22	25.04	24.14	23.16	-	-
Lie et al[20] (2005)	35.62	34.98	33.34	32.43	31.35	-	-
Gur et al[12] (2005)	28.91	27.72	26.10	25.21	24.43	23.98	23.85
Chen et al[7] (2006)	-	28.72	26.12	24.47	-	-	-
Anhari et al[18] (2008)	37.45	36.12	34.82	34.40	31.90	30.91	30.13
Wu et al[19] (2008)	34.07	28.43	27.11	25.16	24.98	-	-
Ma et al[4] (2009)	35.5	34.00	28.12	26.57	24.10	-	-
Proposed	36.52	36.18	35.16	35.04	33.16	33.12	32.28

over radio mobile channel, which we mention at the beginning.

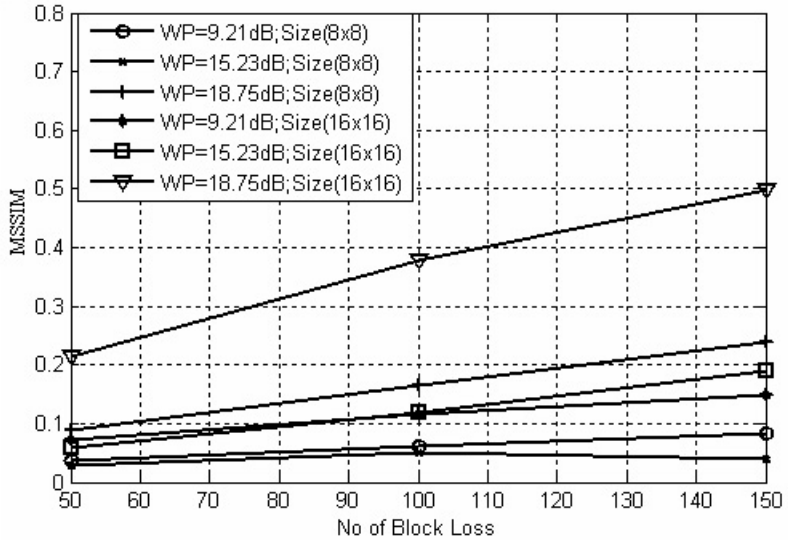

Fig. 24. Relative improvement in MSSIM values after concealment of lost blocks for different watermark power (WP) in dB.

5. Conclusions

An image error concealment scheme based on QIM watermarking is proposed using DTCWT. This scheme provides better capability of error concealment than that of traditional watermarking based method, as DTCWT offers more redundancy than conventional DWT. More number of subbands in DTCWT improves the embedding capacity, which leads to the better reconstruction of the missing data. Moreover, good directional selectivity property of DTCWT offers better reconstruction of edge information of error conceal image. Simulation results show that proposed error

concealment scheme shows better performance of quality improvement even when PLR reaches 30%, compared to that of existing non-data hiding and data hiding based error concealment methods. Simulation results also demonstrate that the proposed scheme provides significant improvement in term of objective evaluations especially for high burst error condition due to fading. Finally, the proposed error concealment scheme can be made use for design of an adaptive data transmission scheme through the estimation of wireless channel condition using the extracted image digest.

Acknowledgments

The authors would like to thank Dr. Nick Kingsbury for providing the software to perform the DTCWT transform operations.

References

1. Y. Wang, and Q. F. Zhu, Error control and concealment for video communication: a review, in *Proc. of the IEEE* **86** (1998) 974–995.
2. S. Aign, and K. Fazel, Temporal and spatial error concealment techniques for hierarchical MPEG-2 video codec, in *Proc. IEEE International Conference on Communications* (1995) 1778–1783.
3. O. Nemethova, A. A. Moghrabi and M. Rupp, Flexible error concealment for H.264 based on directional interpolation, in *Proc. International Conference on Wireless Networks, Communications and Mobile Computing* (2005) 1255–1260.
4. M. Ma, O. C. Au, S. H. G. Chan and M. T. Sun, Edge-directed error concealment, *IEEE Transaction on Circuits and Systems for Video Technology*, **20**(2009) 382–395.
5. H. Sun and W. Kwok, Concealment of damaged block transform coded images using projection onto convex sets, *IEEE Transaction on. Image Processing*, **4** (1995) 470–477.
6. Y. Wang, Q. F. Zhu and L. Shaw, Maximally smooth image recovery in transform coding, *IEEE Transaction on Communications* **41**, (1993) 1544–1551.
7. M. J. Chen, C. S. Chen and M. C. Chi, Recursive block-matching principle for error concealment algorithm, in *Proc. of International Symposium on Circuits and Systems* (2003) 528–531.
8. W. Y. F. Wong, A. K. Y. Cheng and H. S. Horace, Concealment of damaged blocks by neighborhood regions partitioned matching, in *Proc. of International Conference on Image Processing* (2001) 45–48.
9. S. D. Rane, J. Remus, and G. Sapiro, Wavelet-domain reconstruction of lost blocks in wireless image transmission and packet-switched networks, in *Proc. of International Conference on Image Processing* (2002) 309–312.
10. Y. Liu, and Y. Li, Error concealment for digital images using data hiding, in *Ninth DSP Workshop* (2000) 1–6.
11. A. Phadikar, S. P. Maity, M-ary QIM data hiding for error concealment of digital image in JPEG pipeline, in *Proc. of the International Conference on Advances in Computing, Control, and Telecommunication Technologies, IEEE Explore, Kerala, India* (2009) 93–97.
12. G. Gur, F. Alagoz, and M. AbdelHafez, A novel error concealment method for images using watermarking in error-prone channels, in 16^{th} *IEEE International Symposium on Personal, Indoor and Mobile Radio Communications* (2005) 2637–2641.

13. C. K. Nayak, M. Jayalakshmi, S. N. Merchant and U. B. Desai, Projection onto convex sets with watermarking for error concealment, *LNCS* **4815** (2007) 119–127.
14. M. Carli, M. Farias, D. Bailey and S. Mitra, Error control and concealment for video transmission using data hiding, in 5^{th} *International Symposium on Wireless Personal Multimedia Communications, Sheraton Waikiki, Honolulu, Hawaii* (2002) 812–815.
15. C. B. Adsumilli, M. C. Q. Farias, S.K. Mitra and M. Carli, A robust error concealment technique using data hiding for image and video transmission over lossy channels, *IEEE Transactions on Circuits and Systems for Video Technology* **15** (2005) 1394–1406.
16. S. D. Lin, S. C. Shie and J. W. Chen, Image error concealment based on watermarking, in *Proc.* 7^{th} *Digital Image Computing: Techniques and Applications* (2003) 137–143.
17. H. Wang, S. A. Tsaftaris and A. K. Katsaggelos, Joint source-channel coding for wireless object-based video communications utilizing data hiding, *IEEE Transactions on Image Processing*, **15** (2006) 2155–2169.
18. A. K. Anhari, S. Sodagari and A. N. Avanaki, Hybrid error concealment in image communication using data hiding and spatial redundancy, in *Proc. International Conference on Telecommunications* (2008) 1–5.
19. J. Wu, X. Liu and K. Y. Yoo, A temporal error concealment method for H.264/AVC using motion vector recovery, *IEEE Transaction on Consumer Electronics* **54** (2008) 1880–1885.
20. W. N. Lie, T. C. I. Lin, D. C. Tsai and G. S. Lin, Error resilient coding based on reversible data embedding technique for H.264/AVC video, in *Proc. International Conference on Multimedia and Expo* (2005) 1174–1177.
21. P. J. Lee, H. H. Chen and L. G. Chen, A new error concealment algorithm for H.264/AVC video transmission, in *Proc. International Symposium On Intelligent Multimedia, Video, and Speech Processing* (2004) 619–622.
22. S. Mallat, *A wavelet tours of signal processing* (Academic, 1999).
23. P. Abry and P. Flandrin, Multiresolution transient detection, in *Proc. of IEEE SP Int. Symposium time frequency time scale analysis* (1994) 225–228.
24. E. Ozturk, O. Kucur and G. Atkin, Waveform encoding of binary signals using a wavelet and its Hilbert transform, in *Proc. IEEE Int. Conf.Acoust., Speech, Signal Process.* (2000).
25. L. E. Pennec and S. Mallat, Sparse Geometric Image Representation with Bandelets *IEEE Trans. on Image Processing* **14** (2005) 423–438.
26. M. Acharyya and Malay K. Kundu, Extraction of noise tolerant, gray-scale transform and rotation invariant features for texture segmentation using wavelet frames, *International Journal of Wavelets, Multiresolution and Information Processing* **6** (2008), 391–417.
27. D. L. Donoho and M. R. Duncan, Digital curvelet transform: Strategy, implementation and experiments, in *Proc. SPIE* **4056** (2000), 12–29.
28. H. Y. Leung, L. M. Cheng and L. L. Cheng, Robust watermarking schemes using selective curvelet coefficients based on a HVS model, *International Journal of Wavelets, Multiresolution and Information Processing* **8** (2010) 941–959.
29. M. N. Do and M. Vetterli, The finite ridgelet transform for image representation, *IEEE transactions on image processing* **12** (2003) 16–28.
30. Y. Jiang and Y. Liu, Interpolatory curl-free wavelets and applications, *International Journal of Wavelets, Multiresolution and Information Processing* **7** (2007) 843–858..
31. O. J. Lou, X. H. Wang and Z. X. Wang, A new countourlet domain based image watermarking scheme resilient to geometrical attacks , *International Journal of Wavelets, Multiresolution and Information Processing* **7** (2009), 115-130.
32. H.Y. Leung, L.M. Cheng and L.L Cheng, A robust watermarking scheme using se-

lective Curvelet coefficients, *International Journal of Wavelets, Multiresolution and Information Processing* **7** (2009), 163–181.
33. A. Phadikar, S. P. Maity, ROI based quality access control of compressed color image using DWT via lifting, *Electronic Letter on Computer Vision and Image Analysis (ELCVIA)*, **8** (2009), 51–67.
34. C. P. Huang and C. C. Li, Secure and progressive image transmission through shadows generated by multiwavelet transform, *International Journal of Wavelets, Multiresolution and Information Processing* **6** (2008), 907–931.
35. Dejey and R. S. Rajesh, An improved wavelet domain digital watermarking for image protection, *International Journal of Wavelets, Multiresolution and Information Processing* **8** (2010) 19–31.
36. G. Bhatnagar and B. Raman, Distributed multiresolution discrete Fourier transform and its application to watermarking, *International Journal of Wavelets, Multiresolution and Information Processing* **8** (2010) 225–241.
37. S. P. Maity and M. K. Kundu, Performance improvement in spread spectrum image watermarking using wavelets, *International Journal of wavelets, Multiresolution and Information Processing* **9** (2011) 1–33.
38. J. Daugman, Two-dimensional spectral analysis of cortical receptive field profiles, *Vision Research* **20** (1980) 847–856.
39. P. Loo, Digital watermarking using complex wavelets, PhD Thesis, University of Cambridge, 2002.
40. P. Loo and N. Kingsbury, Digital Watermarking Using Complex Wavelets, in *Proc. International Conference on Image Processing* (2000) 29–32.
41. B. Chen, G. W. Wornell, Quantization index modulation: a class of provably good methods for digital watermarking and information embedding, *IEEE Transaction of Information Theory* **47** (2001) 1423–1443.
42. D. Kundur and D. Hatzinakos, Diversity and Attack characterization for improved robust watermarking, *IEEE Transactions on Signal Processing 49* (2001) 2383–2396.
43. N. Kingsbury, Image processing with complex wavelets, *Philosophical Transactions of the Royal Society of London Series A: Mathematical, Physical and Engineering Sciences* **357** (1760) 2543–2560.
44. L. Coria, P. Nasiopoulos, R. Ward and M. Pickering, An access control video watermarking method that is robust to geometric distortions, *Journal of Information Assurance and Security* **2** (2007) 266–274.
45. L. E. Coria, M. R. Pickering, P. Nasiopoulos and R. K. Ward, A video watermarking scheme based on the dual-tree complex wavelet transform, *IEEE Transaction on Information Forensics and Security* **3** (2008) 466–474.
46. T. M. Cover and J. A. Thomas, *Elements of Information Theory* (JohnWiley & Sons, 1991).
47. S. Voloshynovskiy and T. Pun, Capacity security analysis of data hiding technologies, in *Proc. IEEE International Conference on Multimedia and Expo* (2002) 477–480.
48. S. Mabtoul, E. Ibn-Elhaj and D. Aboutajdine, A blind image watermarking algorithm based on dual-tree complex wavelet transform, in *Proc. 2nd International Symposiam On Commucation, Control and Signal Processing* (2006).
49. J. P. Boyer, P. Duhamel and J. B. Talon, Performance analysis of scalar DC-QIM for watermark detection, in *Proc. of IEEE International Conference on Acoustics, Speech and Signal Processing* (2006) II–II.
50. P. W. Wong, Inverse halftoning and kernel estimation for error diffusion, *Media Technology Laboratory*, (1993) 1–23.
51. R. Floyd and L. Steinberg, An adaptive algorithm for spatial grey scale, in *SID In-*

ternational Symposium Digest of Technical Papers (1975) 36–37.
52. *http://www.petitcolas.net/fabien/watermarking/image_database/index.html.*
53. R. C. Gonzalez, R. E. Woods and S. L. Eddins, *Digital image processing using Matlab* (Pearson Education, 2005).
54. Z. Wang, A. C. Bovik, H. R. Sheikh and E.P. Simoncelli, Image quality assessment: from error measurement to structural similarity, *IEEE Transactions on Image Processing* **3** (2004) 1–14.
55. S. P. Maity and M. Mukherjee, Subcarrier PIC scheme for high capacity CI/MC-CDMA System with Variable Data Rates, in *Proc. of IEEE Mobeile WiMAX'09* (2009) 135–140.
56. L. Fang and L. Milstein, Performance of successive interference cancellation in convolutionally coded multicarrier DS/CDMA systems, *IEEE Transactions on Communications* **49** (2001) 2062–2067.
57. W. R. Heinzelman, M. Budagavi and R. Talluri, Unequal error protection of MPEG-4 video transmission, in *Proc. IEEE International Conference on Image Precessing* (1999) 530–534.
58. H. Zhang, J. Wang, Y. Liu, J. Wang and Y. Gao, An efficient two-stage error detector based on syntax and continuity, *IEEE Transactions on Consumer Electronics* **53** (2007) 1276–1280.